Rotorcraft simulation modelling and validation for control law design

B. J. Manimala, D. J. Walker, G. D. Padfield and M. Voskuijl
Department of Engineering
University of Liverpool
Liverpool, UK

A. W. Gubbels
Institute for Aerospace Research (IAR)
National Research Council (NRC) Canada
Ottawa, Ontario
Canada

ABSTRACT

This paper describes the development and validation of a high fidelity simulation model of the Bell 412 helicopter for handling qualities and flight control investigations. The base-line model features a rigid, articulated blade-element formulation of the main rotor, with flap and lag degrees of freedom. The Bell 412 HP engine/governor dynamics are represented by a second-order system. Other key features of the base-line model include a finite-state dynamic inflow model and lag damper dynamics. The base-line model gives excellent agreement with flight-test data over the speed range 15-120kt for on-axis responses. Prediction of off-axis responses is less accurate. Several model enhancement options were introduced to obtain an improved off-axis response. It is shown that the pitch/roll off-axis responses in transient manoeuvres can be improved significantly by including wake geometry distortion effects in the Peters-He finite-state dynamic inflow model.

NOMENCLATURE

C_{eq}	non-dimensional lag damper coefficient
C_ζ	lag damping
d	lag damper spindle arm length
e_β	flap hinge offset ratio
e_ζ	lag hinge offset ratio
I_β	flap moment of inertia with respect to the flap hinge
I_ζ	lag moment of inertia with respect to the lag hinge
K_β	flap hinge spring stiffness
K_ζ	lag hinge spring stiffness
$K_{\zeta,f}$	stiffness provided by the flexi-beam at the yoke of a hingeless rotor
K_{eq}	non-dimensional stiffness
k_1,k_2	gains in the engine model
$m(r)$	blade mass/unit length distribution
M_ζ	damper moment about the lag hinge
M_β	first mass moment with respect to the flap hinge

Paper No. 3123. Manuscript received 2 August 2006, accepted 21 November 2006.

https://doi.org/10.1017/S0001924000001780 Published online by Cambridge University Press

M_ζ	first mass moment with respect to the lag hinge
p, q, r	fuselage angular velocities in body axis
Q_e	engine output torque
R	rotor radius
r_e	blade element radial location
TAS	true airspeed measurement
u, v, w	body axis velocities at the aircraft centre of gravity
u_0,v_0,w_0	trim values of the body axis velocities
u_w,v_w,w_w	component of wind velocities.
w_f	fuel flow change

Greek Notation

α	angle-of-attack
β	angle of side-slip
ζ	lag angle
θ	pitch attitude
λ_β	first flap frequency ratio
λ_ζ	first lag frequency ratio
T_1,T_2	engine time constants
φ	bank angle
ψ	blade azimuth angle
Ω	main rotor rotational speed
ω	Frequency

1.0 INTRODUCTION

The Helicopter Active Control Technology (HELI-ACT) research project being conducted at the University of Liverpool aims to develop advanced control system concepts for helicopters using modern modelling and multivariable control techniques. The project consists of a combined theoretical and experimental investigation using state-of-the-art simulation and control tools. The main aims of the project are to develop a better understanding of the issues relating to helicopter modelling, identification and control and to develop new control concepts for mutual satisfaction of handling qualities, flight envelope protection and load alleviation requirements. The project involves collaboration with The National Research Council (NRC) of Canada and utilises the six-axis motion flight simulator at the University of Liverpool[1] and the NRC Bell 412 Advanced Systems Research Aircraft (ASRA)[2] shown in Fig. 1. Use of the highly instrumented ASRA, including rotor blade instrumentation, will enable the investigation of some of the deficiencies in existing mathematical models. Better control systems, designed more quickly and with less trial-and-error and flight-test development will be achievable if the complexity of the helicopter's dynamics can be accurately modelled and taken into account. A key aspect of the HELI-ACT project has been the development in the comprehensive real-time simulation programme FLIGHTLAB[3] of a high-fidelity simulation model of the Bell 412 ASRA. This paper, a preliminary version of which was presented at the 31st European Rotorcraft Forum, Florence, Italy, in September 2005, describes the development and validation of that model.

The Bell 412 HP is a twin-engined 1,800shp utility helicopter with a four-bladed fibreglass main rotor and a maximum take-off weight of 11,900lb. In 1993, NRC acquired a Bell 412 HP for use as an airborne simulator vehicle. Evaluation of the aircraft confirmed that it had many of the desirable attributes of an airborne simulator, including high control response bandwidth and high control power. The NRC ASRA is a highly modified version of the Bell 412 HP. One of the most notable modifications has been the addition of a full-authority programmable digital flight control system which enables experimental control algorithms to be flight-tested.

An accurate representation of the flight dynamics of a helicopter requires, amongst other things, a reliable set of configuration data comprising vehicle aerodynamic, structural/inertial and geometric details. A large amount of the modelling effort in this project consisted of data collection, partly from the public domain (published papers and technical reports) and partly from measurements carried out at the NRC. When data were not available, estimates based on engineering judgement were made, so that the simulation predictions produced a good agreement with the flight-test data. This is discussed later in the paper.



Figure 1. The NRC Bell 412 Advanced Systems Research Aircraft.

2.0 OVERVIEW OF THE MODEL

2.1 Bell 412 rotor hub design

The Bell 412 hub (Fig. 2) is a hingeless design in which the blades are attached to the hub through flexible titanium yokes, known as flexures or flexi-beams[4]. The flexures are designed to give an equivalent flap-hinge offset that affords good control response but minimises gust responses and oscillatory hub moments transmitted to the fuselage. The blade lag and pitch motions take place about conical/spherical bearings that also retain the blades and transmit centrifugal forces to the yoke. The rotor configuration is described as a soft in-plane, the first in-plane mode being below the 1/rev frequency. Blade lag damping is provided by two identical elastomeric pads, which are housed in bridges that attach to the upper and lower sides of the yoke.

The baseline FLIGHTLAB simulation model of the Bell 412 (designated F-B412) features a rigid, articulated, blade-element rotor formulation with flap and lag degrees of freedom. Spring strengths and locations were chosen to match the first flap and lag frequencies quoted in Refs 4 and 5. The normalised frequencies of the first six rotor modes as quoted in Ref. 4 are summarised in Table 1. According to Ref. 4, the boundary conditions used in calculating these frequency ratios are cantilevered for the out-of-plane motion and pinned for the in-plane motion, and the control system stiffness is represented in the torsional boundary condition.



Figure 2. NRC Bell 412 hub.

https://doi.org/10.1017/S0001924000001780 Published online by Cambridge University Press

Table 1
Rotor frequency ratios for the Bell 412[4]

Mode	Frequency ratio (ω/Ω)
1st lag	0·6-0·7
2nd lag	3·13
1st flap	1·03
2nd flap	2·59
3rd flap	4·47
1st torsion	5·15

Another key feature of the baseline model is the inclusion of lag dynamics. The inflow model used is the enhanced Peters-He finite-state dynamic inflow model[6]. As will be shown, the baseline model produced good on-axis responses in comparison to the flight-test data over the speed range 15-120kt. However, off axis responses were less satisfactory. Several model enhancement options available in FLIGHTLAB were then introduced to obtain improved off-axis response. The enhancements included modelling of the rotor inflow dynamics in manoeuvres with wake distortion and rotor wake interference on other surfaces, such as the fuselage and horizontal tail. It will be shown later in this paper that the roll/pitch off-axis responses in transient manoeuvres can be improved by including the wake geometry distortion effect in the Peters-He finite-state dynamic inflow model.

2.2 Modelling of the Bell 412 hub and blade retention

Reference 7 discusses different ways of modelling various types of blade flap retention systems. A fully-coupled elastic model representing the flap, lag and torsional degrees of freedom is, in principle, the most accurate way of modelling a hingeless rotor. However, in order to create such a model it is necessary to know the flap, lag and torsional stiffness and mass distributions, and the location of the flexural axis of the blade along its span. As information on the blade structural properties was not available, a rigid-blade model with equivalent offset hinge and spring stiffness was deemed to be the next most appropriate model for the elastic deformation of a moderately stiff hingeless rotor blade.

With a first flap mode frequency ratio of 1·03, the Bell 412 rotor system is also relatively 'soft' out-of-plane (i.e. in flap), hence an offset hinge and spring model is a reasonable approximation. For the FLIGHTLAB modelling of the Bell 412, the hub is modelled by using separate flap and lag hinges and springs whose parameters were chosen in such a way that the first flap and lag frequencies matched those of Table 1.

2.3 Selection of flap hinge parameters

The following value for the flap hinge offset ratio is quoted in Ref. 8.

$$e_\beta = 0\cdot 046$$

This is based on the assumption that the effective flap hinge is coincident with the pitch bearing. Given the above, the spring constant for the flap hinge can be obtained by matching the frequency ratio of the first mode in the flap degree of freedom.

The expression for the first flap frequency ratio (λ_β) for the flap motion, assuming decoupled modes, is given by[7]:

$$\lambda_\beta^2 = 1 + \frac{K_\beta}{I_\beta \Omega^2} + \frac{e_\beta R}{I_\beta} M_\beta \qquad \ldots (1)$$

in which

$$I_\beta = \int_{e_\beta R}^{R} \left(r_e - e_\beta R\right)^2 m(r_e)\mathrm{d}r_e$$

is the flap moment of inertia with respect to the flap hinge and

$$M_\beta = \int_{e_\beta R}^{R} \left(r_e - e_\beta R\right) m(r_e)\mathrm{d}r_e$$

is the first mass moment with respect to the flap hinge offset.

The blade mass distribution $m(r_e)$ is required for evaluating the above moment integrals. The Bell 412 blade mass distribution was modelled using the mass distribution given in Ref. 9, scaled so as to match the known mass of the Bell 412 blade.

The spring stiffness K_β giving the first flap frequency ratio λ_β = 1·03 is obtained from Equation (1). Numerical values of these parameters can be found in Appendix A. It will be noted that the spring stiffness is negative. The yoke, which is flexible in flap, provides a virtual flap hinge inboard of the pitch bearing.

2.4 Equivalent lag hinge stiffness

This section describes how the lag hinge stiffness and damping values were obtained for the F-B412. The blade lag and pitch change motions take place on a conical/spherical bearing that also retains the blade[4]. According to Ref. 8, this bearing is located at 9·3% of the rotor radius from the hub-centre, giving a lag hinge offset ratio of

$$e_\zeta = 0\cdot 093$$

The expression for the first lag frequency ratio (λ_ζ) for the lag motion is given by:

$$\lambda_\zeta^2 = \frac{e_\zeta R}{I_\zeta} M_\zeta + \frac{K_\zeta}{I_\zeta \Omega^2} \qquad \ldots (2)$$

in which the lag moments I_ζ and M are defined analogously to their flap counterparts in Equation (1). A spring stiffness K_ζ = 127,700ft-lb/rad gives the required non-dimensional lag frequency of λ_ζ = 0·65.

2.5 Linear Lag damper model

The blade lag damping for the Bell 412 is provided by two identical elastomeric dampers. The modelling of elastomeric lag dampers is an important area of research in its own right, due to the complexity of the changes in material properties with operating conditions[8]. The properties of the elastomeric materials depend on strain amplitude and temperature. In addition to strain amplitude dependence, elastomeric materials also exhibit frequency dependence. The frequency of the first lag mode depends on the stiffness of the damper, which in turn depends strongly on the instantaneous strain amplitude in the elastomer. Reference 8 describes various modelling methods, which effectively capture the material behaviour for a range of strain amplitudes and frequencies, representative of the operating conditions of helicopter elastomeric dampers.

FLIGHTLAB provides a spring-damper component to model the lag dampers. The damping can be either constant, viscous damping, or it can be defined in a hysteretic frequency-dependent form. Currently, the viscous lag damper option is chosen for the F-B412 model. To obtain the damping constant for the model, the following theory for elastomeric damping was used[8]. The damper displacement x is related to the lag angle ζ (assumed small) through the spindle arm length d by the following equation:

$$x = d\zeta \qquad \ldots (3)$$

The damping moment about the lag hinge can be written as

$$\text{Damping moment} = \left(K'x + \frac{K''}{\omega}\dot{x}\right) \times d = \left(K'd^2\zeta + \frac{K''d^2}{\omega}\dot{\zeta}\right) \qquad \ldots (4)$$

https://doi.org/10.1017/S0001924000001780 Published online by Cambridge University Press

in which the term $K''d^2$ is the equivalent viscous damping at the frequency ω. A value for this parameter was deduced from Ref. 8, where the equivalent non-dimensional stiffness and damping coefficients of two different damper configurations are plotted as a function of lag angle. The term $K'd^2$ is the stiffness provided by the damper. The total stiffness K_ζ for the lag motion is

$$K_\zeta = K'd^2 + K_{\zeta f} \quad \ldots (5)$$

where $K_{\zeta f}$ is the stiffness provided by the flexi-beam at the yoke. According to Ref. 8, the stiffness contribution from the flexi-beam is of order 2% of the contribution from the damper. The value of K_ζ is obtained by matching the first lag frequency.

The non-dimensional stiffness and damping coefficients are defined as:

$$K_{eq} = \frac{K'd^2}{I_\zeta \Omega^2}, \quad C_{eq} = \frac{K''d^2}{\omega I_\zeta \Omega} \quad \ldots (6)$$

Using a non-dimensional damping coefficient of 0·075 based on Ref. 8, the damping term $K''d^2/\omega$ is obtained as:

$$\frac{K''d^2}{\omega} = 0{\cdot}075 \times I_\zeta \Omega = 1{,}467{\cdot}6 \ \ ft - lbf - s - rad^{-1}$$

Since there are two elastomeric dampers per blade for the Bell 412 rotor, the damping value used for the FLIGHTLAB damper component is twice the above value:

$$C_\zeta = 2{,}935{\cdot}2 \ \ ft - lbf - s - rad^{-1}$$

Note that, in the model, the damping coefficient remains constant. In practice, this will not be the case, because in forward flight, the combined 1/rev and harmonics will reduce the damping. This is known as a dual frequency effect[8].

3.0 BLADE AERODYNAMICS

In the baseline model, each blade is divided into several aerodynamic segments and each segment is treated as a two-dimensional panel producing aerodynamic loads as non-linear functions of angle of attack, dynamic pressure and Mach number. A quasi-steady aerodynamic component was used for the air load calculation on the blade elements. The blade aerodynamic segments are defined based on the equal annuli area approach. This means that the segments become shorter towards the tip of the blade. The aerodynamic loads are calculated by treating the blade sections as two-dimensional panels. The 2D aerofoil table stores lift, drag and pitching moment coefficients as functions of angle of attack and Mach number.

3.1 Aerofoils

According to Ref. 4, the Bell 412 blade contains two aerofoils - the BHT 674 for the inner sections and Wortmann FX-080 towards the tip. The FX-080 aerofoil is believed to be a modified version of either the Wortmann FX-71-H-080 or the FX-69-H-080 (8% thick with a slight camber). Due to lack of detailed information on these aerofoils, VR7 aerofoil data[10,11] were used as a substitute for the BHT 674 and data for a 9% thick cambered aerofoil (OA309 aerofoil) were used for the tip aerodynamic segments. The aerofoil data were represented in table look-up form with lift, drag and pitching moment coefficients tabulated against angle-of-attack (–180 to 180deg) and Mach number (0-0·9 Mach).

3.2 Inflow model

Rotor inflow modelling has been an area of extensive research over the past three decades. Considerable progress has been made in this area, starting from the classical actuator disk theory in which the inflow of air is assumed to be uniform over the rotor disk. More recent developments include dynamic inflow models which account for low-frequency wake effects under transient conditions. Among various rotor wake solutions, the Peters-He finite-state dynamic wake model[6] and the distorted vortex wake models, such as described in Refs. 12, 13, and 14, represent major advances in practical rotor wake analysis/simulation technology.

The Bell 412 model described in this work makes use of the Peters-He finite-state dynamic wake model. This model attempts to capture the uniform and first harmonic distribution of the inflow and the transient response of these inflow components in manoeuvring flight. This methodology also models the dynamic response of the inflow to manoeuvring flight and predicts the off-rotor components of inflow for use in interference modelling at the fuselage and tail.

4.0 TAIL ROTOR

FLIGHTLAB's Bailey rotor component is used to model the tail rotor. The Bailey rotor model is based on the analysis described in Ref. 15. In the Bailey model, closed form expressions for rotor thrust and torque are obtained analytically by integrating the air loads over the rotor blade span and averaging them over the azimuth. Only rotor coning is considered and hence there is no provision for blade cyclic pitch inputs. The induced velocity is computed from a uniform inflow model. The following assumptions are employed in the derivation of the tail rotor equations:

1. Constant chord and linear twist
2. Linear lift with lift curve slope
3. Incompressible flow
4. No individual blade dynamics, except for the steady state coning.
5. Uniform induced flow over the rotor

5.0 FUSELAGE

There are several modelling options available within FLIGHTLAB for the fuselage aerodynamics, including a panel method and a simple table look-up. For the Bell 412 model, the table look-up option was chosen where the fuselage coefficients are supplied by means of look-up tables as functions of angle of attack and sideslip angle.

Several sources were used to estimate the fuselage aerodynamic characteristics of the Bell 412. Reference 16 gives some information about the longitudinal aerodynamic coefficients for several fuselages of Bell helicopters. However, the data are incomplete; for example, the body drag polar trend has been referenced to minimum drag and thus only represents the increment in drag due to angle of attack. This drag increment, which includes hub and landing gear, has been normalised by projected frontal area and dynamic pressure. Reference 17 reports the results from the wind-tunnel tests of two full-scale helicopter configurations conducted at the NASA Ames 40 by 80 foot Wind Tunnel facility. For the wind-tunnel tests, a full-scale mock up of a lightweight observation helicopter (LOH) served as one test vehicle and a medium weight utility class helicopter (MUH) served as the other. The LOH was a full-scale mock up the Bell HO-4, built with production construction techniques; the MUH was a Bell UH-1 helicopter.

Data from Ref. 18 were used for the side force and yaw moment coefficients of the F-B412 fuselage model. This NASA report presents the results of the wind-tunnel investigation of three different

https://doi.org/10.1017/S0001924000001780 Published online by Cambridge University Press

fuselage models in the presence of a rotor wake. These models represented three helicopters widely used by the US Army. Out of the three fuselage models tested, the second wind-tunnel model was a scaled version of the Bell UH-1 helicopter. Forces and moments of the fuselage and the rotor were measured at wind speeds of up to 102 knots through ±180deg of sideslip.

6.0 HORIZONTAL STABILISER

The Bell 412 uses an inverted Clark-Y aerofoil for the tail section[19, 20] with a Gurney flap fitted on the trailing edge. The stabiliser is attached to a spring-loaded tube so that the incidence is determined by the aerodynamic pitching moment and the spring rate. The exact location of the elevator and its dimensions were obtained from Ref. 20. For the NRC Bell 412, the left and the right elevator have different incidences. It was determined by the NRC (Ref. 19) that the left and right elevators have incidences of 5·6° and –2·4° respectively. The spring constant was determined by NRC by applying known moments to the stabiliser and recording the angular displacement.

The lift and drag coefficients of the Clark-Y aerofoil are obtained from Ref. 21. The data given[21] were obtained from wind tunnel experiments on a full-scale wing of aspect ratio 4. The experiment covered a large range of angle-of-attack (–45° to +90°). Higher angle approximations were used to obtain the lift and drag coefficients outside this range. The effect of the Gurney flap was modelled by modifying the aerodynamic data to incorporate the change in pitching moment and lift curve slope. The horizontal stabiliser spring is modelled by the use of a FLIGHTLAB spring-damper component.

7.0 VERTICAL FIN

The location and dimensions of the vertical fin were obtained from Ref. 20. The aerodynamic characteristics of the fin aerofoil are not known at this point and hence it was decided to use the UH60 fin aerodynamic data. The UH60 uses a modified NACA 0021 aerofoil for its fin section. Reference 22 gives the lift and drag polar of this aerofoil for a range of –90° to 90° angle of side-slip. For the F-B412 implementation, these data were extended to the range –180° to 180°.

8.0 ENGINE DYNAMICS

The NRC has developed a linear state-space model of the Bell 412 engine-governor-rotorspeed dynamics, based on frequency domain system identification from flight-test data[23]. The model was designed to capture the fuel flow, gas turbine speed, power generator speed and engine output torque dynamics in response to collective input. The input to the model is collective lever displacement relative to trim. NRC included five states in the model structure and a delay on the input. The model parameters were identified at hover and 60kt. The torque response of the model closely matches that of the ASRA, characterised by an essentially second-order dynamic.

The task was to incorporate this linear model into the F-B412 non-linear model. FLIGHTLAB offers several options to model an engine, including a simple engine model (Ref. 7). The simple engine model functions like an engine governor. It commands torque based on the difference between the current rotor speed and the rotor idle speed. The engine output torque is controlled by the governor system that senses a change in rotor speed ($\Delta\Omega$) and demands a fuel flow change (w_f). The fuel change is represented as a first order lag.

$$\tau_1 \dot{w}_f + w_f = k_1 \Delta\Omega \quad \ldots (7)$$

where τ_1 and k_1 are the time constant and the gain, respectively. The gain k_1 can be chosen to give a prescribed droop in rotor speed from flight idle to maximum contingency fuel flow. The engine torque (Q_e) response to the fuel flow change is described by a lag responding to fuel flow and flow rate.

$$\tau_3 \dot{Q}_e + Q_e = k_2(\tau_2 \dot{w}_f + w_f) \quad \ldots (8)$$

where k_2 is the gain and $\tau 2$ and $\tau 3$ are the time constants. Combining the above first order equations gives the second order equation :

$$\tau_1\tau_3 \ddot{Q}_e + (\tau_1 + \tau_3)\dot{Q}_e + Q_e = k_1 k_2[\Delta\Omega + \tau_2 \dot{\Omega}] \quad \ldots (9)$$

The time constants and gains of the simple engine model were tuned to match the response of the NRC state space engine model in hover.

The response to a collective step input from the NRC linear engine model and from the FLIGHTLAB Bell 412 simple engine model are shown in Fig. 3. Also displayed is the response of a linear second-order system with natural frequency of 0·53rad/s and damping ratio of 0·11 for the same input. The collective time delay was approximated using a 3rd order Padé approximation. The engine torque response of the F-B412 with simple engine model matches that of the NRC linear model well.

Figure 4 shows the response of the F-B412 model to a 2-3-1-1 collective input at a true air speed (TAS) of 18kt. Flight-test data (denoted 'Meas') showing the responses of the ASRA in flight are superimposed. It is seen that the predicted mast torque matches the measured data well. Also shown are rotor speed (normalised with the trim rotor speed) and climb rate, which also show reasonable correlation. The comparisons shown in Fig. 4 demonstrate the ability of the model to capture the salient heave and engine dynamics.

9.0 AERODYNAMIC INTERFERENCE

Modelling the aerodynamic interactions is a challenging aspect of rotorcraft simulation. A commonly used and effective way of interactional modelling is by incorporating look-up tables representing the downwash/up-wash velocities at the respective aerodynamic surfaces, defined by the values of loads on the generating surface. In the absence of empirical/experimental data, the off-rotor induced velocity predicted by FLIGHTLAB's inflow model is used for the

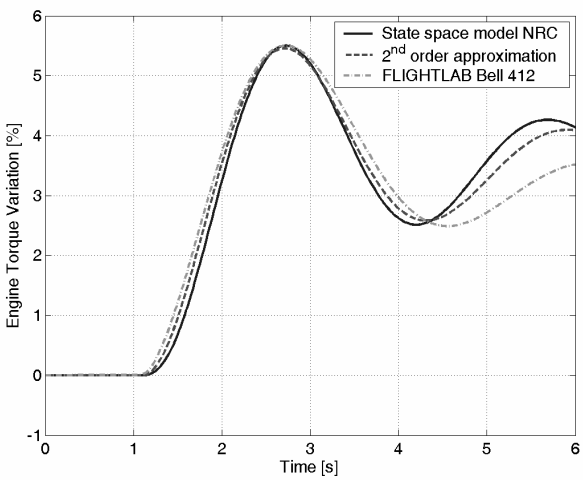


Figure 3. Engine torque response to a collective step input.

https://doi.org/10.1017/S0001924000001780 Published online by Cambridge University Press

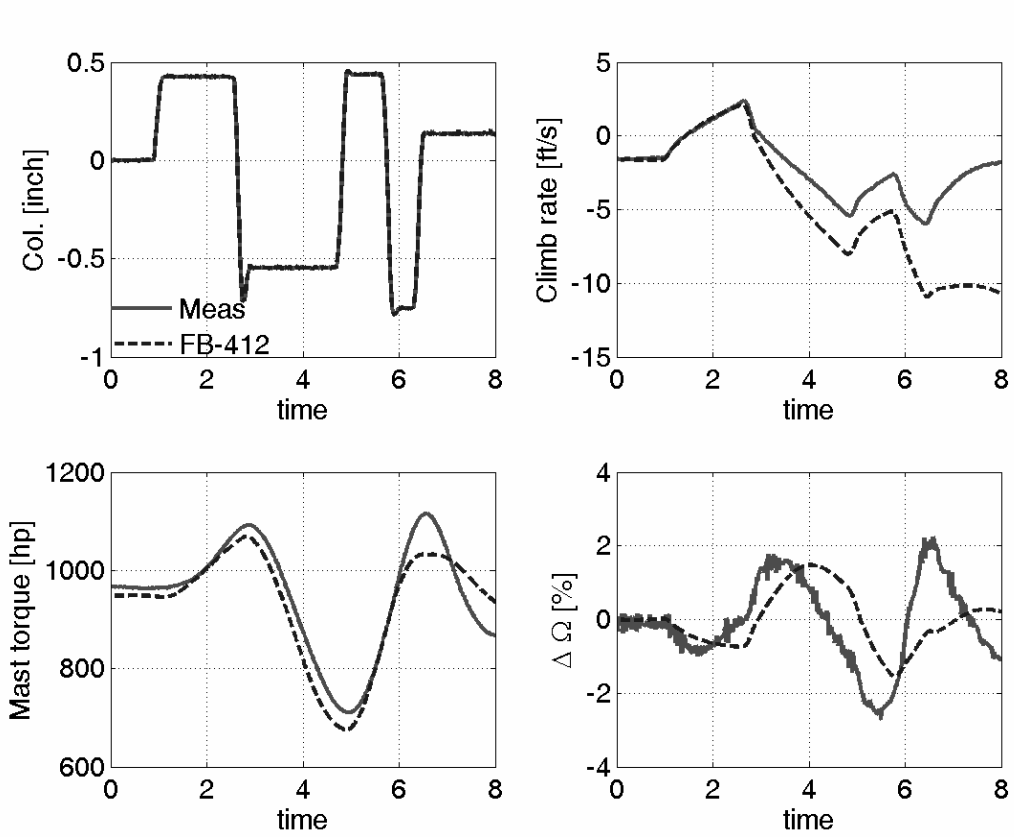


Figure 4. Mast power, rotor speed and rate of climb (18kt TAS).

calculation of the effect of the main rotor wake on fixed aerodynamic surfaces. From the finite-state dynamic wake equations, the induced velocity at an arbitrary flow field point can be computed[24]. The base-line F-B412 model utilises this finite-state dynamic interference model for the main rotor wake effects. The main rotor wake interference is applied to both the empennage and the fuselage.

10.0 MASS AND INERTIA PARAMETERS

Aircraft operating weights and CG position can be reasonably accurately determined at the start of any flight. However there were no data available on the mass moments of inertia of the aircraft. The ASRA is a heavily instrumented research aircraft, and it is supposed that its moments of inertia are appreciably higher than those of the standard Bell 412 HP. For the F-B412 model, the inertia terms were manually tuned by trial and error until the simulation model gave similar short term roll, pitch and yaw responses to the test data.

11.0 MODEL VALIDATION AGAINST FLIGHT-TEST DATA

The baseline F-B412 model was calibrated against flight-test data supplied by NRC Canada. The ASRA's ring laser gyro inertial system (LTN-92) provided accelerations, rates and attitudes. The LTN-92 uses three ring laser gyros, force rebalanced accelerometers and three high-speed microprocessors[25]. The inertial positions and velocities are measured using a NovAtel differential GPS system. The body axis aircraft velocities are computed by transforming the earth fixed inertial velocities (GPS measurements) using Euler transformations. A detailed description of the ASRA data acquisition system can be found in Refs 25 and 26.

The data contained 2-3-1-1 type inputs at low (around 15kt), medium (around 60kt) and high (90-120kt) speeds with the stability augmentation system (SAS) switched off. In addition, certain trim data were available. The data included pilot stick positions, which had to be converted to blade pitch angles, in order to facilitate a direct flight mechanics comparison. NRC made measurements on the aircraft enabling the mechanical gearings between the pilot control position and the resulting blade pitch motion to be calculated, thus enabling the mechanical control system of the Bell 412 to be represented in FLIGHTLAB. Finally, the actuation was modelled as first-order lags with 17Hz bandwidth.

11.1 Trim

F-B412 trim attitude predictions are plotted alongside in-flight measurements in Fig. 5. The flight data are compared with predictions for the baseline F-B412 model with and without interference

https://doi.org/10.1017/S0001924000001780 Published online by Cambridge University Press

effects of the main rotor wake on the fuselage and the empennage. The pitch attitude predicted using the rotor interference on the horizontal stabiliser and fuselage shows better agreement, particularly at speeds up to 40kt. However, at higher speeds there are larger differences between the measured and predicted values. The errors may be due to incorrect fuselage drag, modelling deficiencies in the horizontal stabiliser, or to variations in sideslip affecting the trim flight-test data. (The simulation tests were at zero sideslip.)

Figure 6 shows the main rotor mast power predicted by the F-B412 models and the measured values. There is good agreement for speeds up to 80kt. This suggests that the aerodynamic characteristics of the aerofoils used in the F-B412 model are a reasonable representation of the real Bell 412 blades. At higher speeds, when portions of the rotor disc are more heavily loaded, it is more difficult to predict the power accurately because accurate blade aerodynamic data is required at higher Mach numbers; drag divergence and the associated drag increase may need to be more accurately represented.

Unsteady aerodynamics, dynamic stall and 'stall delay', whereby the boundary layer change caused by rotor rotation adds 3D effects to the blade unsteady aerodynamics, may also be contributory factors. FLIGHTLAB allows unsteady blade aerodynamics and 3D stall delay effects to be modelled. From Fig. 6, it can be seen that the inclusion of the quasi-unsteady blade aerodynamics with stall delay slightly improves the power prediction at higher speeds.

11.2 Dynamic response

This section gives a comparison between the responses predicted by the F-B412 and flight-test data at 35kt TAS. Figures 7 and 8 are the time histories of the pilot control positions and the aircraft states from flight test data recorded at 35kt TAS.

A kinematics consistency analysis of the flight-test data revealed that the helicopter was trimmed with a substantial amount of body axis lateral velocity (about 50ft/s). Such a trim condition was attributed to a side wind encountered by the helicopter during the flight-test. The wind velocities were not directly available from the flight-test data. However, measurements of the angle of attack, angle of side-slip and true air speed were available. Figure 9 shows these measurements during part of the longitudinal manoeuvre. The expressions for the angle-of-attack, side slip angle and the true airspeed are given below:

$$\alpha = \mathrm{Tan}^{-1}\left(\frac{w+w_w}{u+u_w}\right) \quad \ldots (10)$$

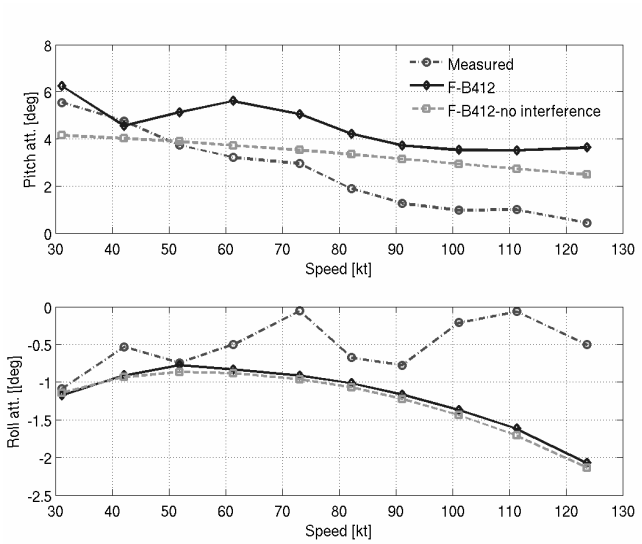


Figure 5. Trim attitudes – predicted and measured.

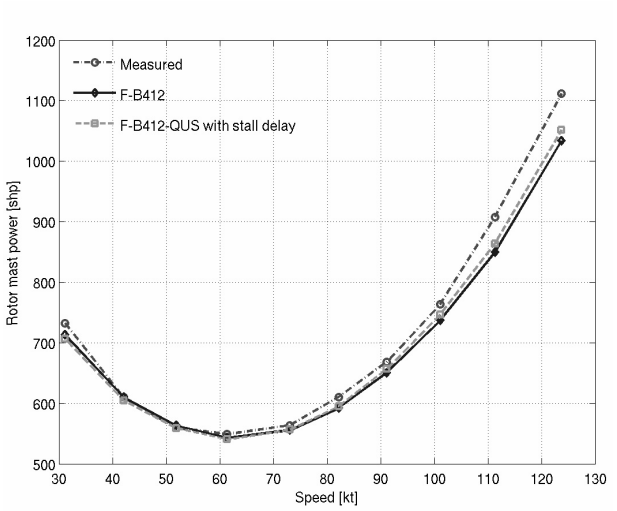


Figure 6. Main rotor mast power – measured and predicted.

$$\beta = \mathrm{Tan}^{-1}\left(\frac{v+v_w}{u+u_w}\right) \quad \ldots (11)$$

$$TAS = \sqrt{(u+u_w)^2+(v+v_w)^2+(w+w_w)^2} \quad \ldots (12)$$

where u_w, v_w and w_w are the wind velocity components. The wind velocity components are expressed in wind axis system as illustrated in Appendix B.

Using angle-of-attack, side-slip, TAS, u, v, and w, the wind velocities were estimated by solving Equations (10)-(12). The estimated steady wind velocities during part of the longitudinal manoeuvre are shown in Fig. 10.

Therefore, before applying the control perturbations, the F-B412 model was trimmed with the velocity components given in Table 2.

It should be noted that the flight-test was conducted at a barometric altitude of around 3,000ft, where a steady wind of 37kt would not be unusual.

The comparison of the F-B412 responses against the flight-test data for a longitudinal input is shown in Fig. 11. The on-axis pitch responses (q, θ) show good agreement between the flight-test data and the F-B412 model. The predicted cross-coupling into roll (p, φ) shows the correct trend, although peak magnitudes differ.

The simulation model appears to under-predict the cross-coupling into yaw (r) for longitudinal input at this flight

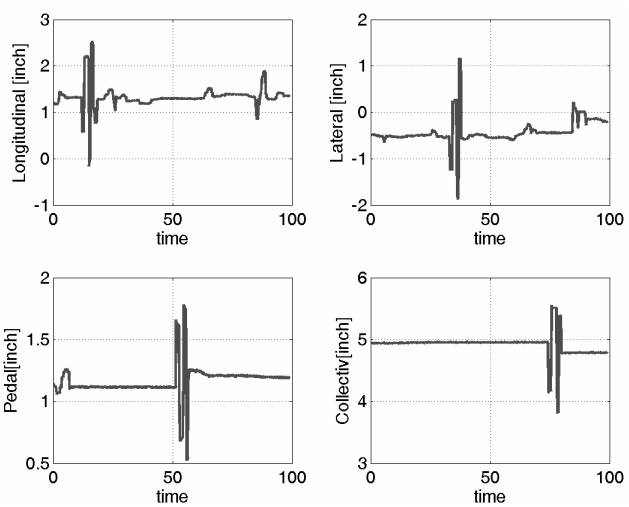


Figure 7. NRC Bell 412, Flight-test data TAS 35kt, control positions.

https://doi.org/10.1017/S0001924000001780 Published online by Cambridge University Press

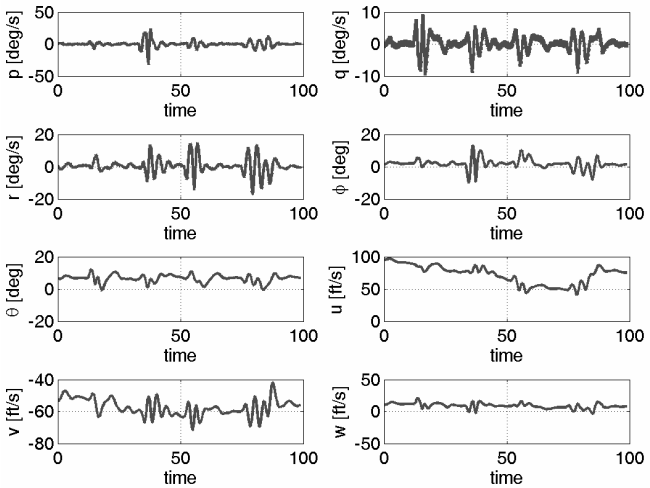


Figure 8. NRC Bell 412, Flight-test data TAS = 35kt, Aircraft States.

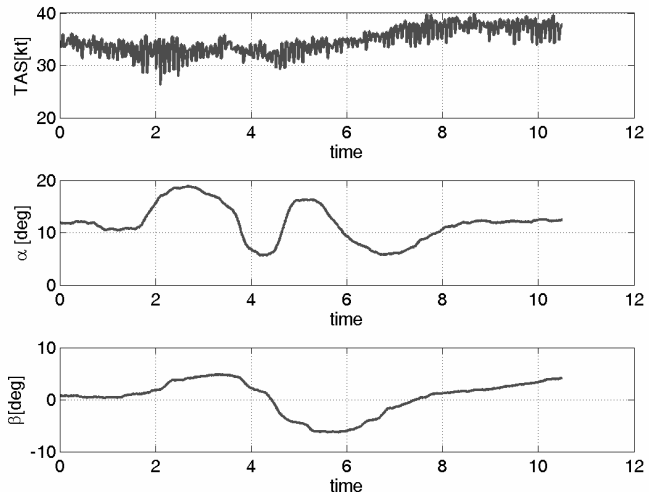


Figure 9. True airspeed, angle of attack and side slip angle during the longitudinal manoeuvre.

condition. The phugoid like mode, indicted by the states w and θ, is well predicted by the model. Response of the body axis longitudinal and lateral velocities matches u and v initially and then starts to deviate.

Figure 12 gives the comparison between the model and flight-test for a lateral stick input, also at 35kt TAS. Once again, there is excellent agreement as far as the on-axis response (p, φ) is concerned. The prediction of the pitch-to-roll coupling is also good, but the model significantly under-predicts roll-to-yaw cross-coupling.

Figure 13 shows the responses of the model and the helicopter to a pedal input. The model predicts the peak yaw rate accurately but the yaw damping is over-predicted. The cross-coupling into roll is fairly well predicted, as are the general trends on the body-axis velocity components.

Figure 14 shows the response to a 2-3-1-1 input on collective. The differences in body axis velocities (especially w) for this flight condition are possibly attributable to errors in the initial trim attitudes. The roll, pitch and yaw rate responses all show correct trends. Referring back to Fig. 4 it may be seen that for a collective input, the simulation model predicts the mast-power and climb-rate well, albeit at a slightly lower speed.

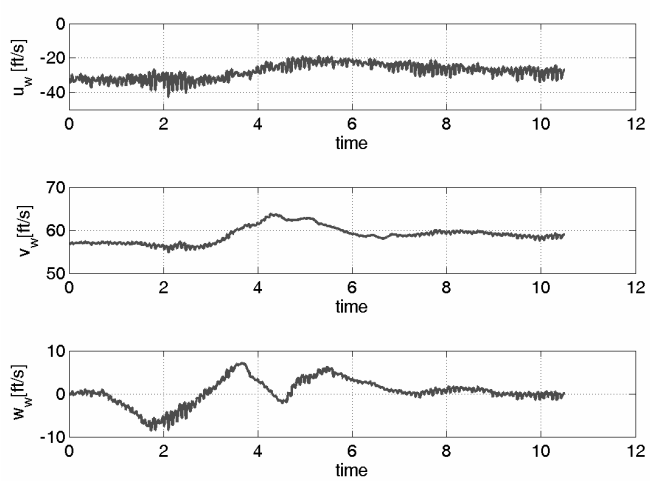


Figure 10. Computed wind velocities in body axis for longitudinal manoeuvre.

11.3 Discussion of off-axis responses

Blade-element based helicopter simulation models generally seem to have difficulties predicting off-axis responses (e.g. roll response to a pitch input and pitch response to a roll input). Indeed, models often predict the off-axis angular rates in the wrong direction. The problem has received attention in the literature[27-30]. One school of thought is that when the rotor tip-path plane tilts due to the application the cyclic control, the rotor wake distorts in a dynamic fashion, resulting in an induced velocity variation over the rotor disk. Various models have been applied to describe the distortion of the rotor wake in transient manoeuvre flight, caused by the applied moments and the rotor passing closer to the blade tip vortices. Comprehensive vortex methods may be capable of better capturing the off-axis response, since they include the distortion of the wake due to angular motion of the tip-path plane[31,32]. For the present, it is difficult to see how such formulations, involving considerable additional complexity, could be incorporated into the type of flight mechanics models required for controller design and handling qualities investigations, especially those required to run in real-time. Furthermore, in recent years, progress has been made towards correcting the off-axis response in flight mechanics simulation models using empirical corrections. Introducing an aerodynamic phase lag and applying a correction factor to the dynamic inflow are two such methods[29]. An alternative approach[30] is to resolve the deficiencies in off-axis response and aerodynamic interaction through improvement of the Peters-He finite-state dynamic wake model. In this approach, the rotor wake distortion effects are accounted for 'on-line' in the rotorcraft simulation code's finite-state dynamic inflow model via influence coefficients calculated off-line using a manoeuvre vortex wake model. The enhanced finite-state dynamic wake model considers the transient wake distortion and inherently addresses the source of the off-axis rotor moments, while providing a computationally more efficient approach than a vortex wake model. The approach of Ref. 30 has been integrated into the F-B412 model.

Figure 15 shows the effect on the off-axis response of including the wake distortion effect in the finite-state dynamic inflow model for a roll input at around 18kt TAS. It can be seen that the model without the wake distortion effect predicts a pitch rate response in

Table 2
Computed trim velocities at start of longitudinal manoeuvre

u_0	v_0	w_0	u_{w0}	v_w	w_{w0}
89·1ft/s	–52·134ft/s	11·8ft/s	–33·25ft/s	52·94ft/s	0·03ft/s

https://doi.org/10.1017/S0001924000001780 Published online by Cambridge University Press

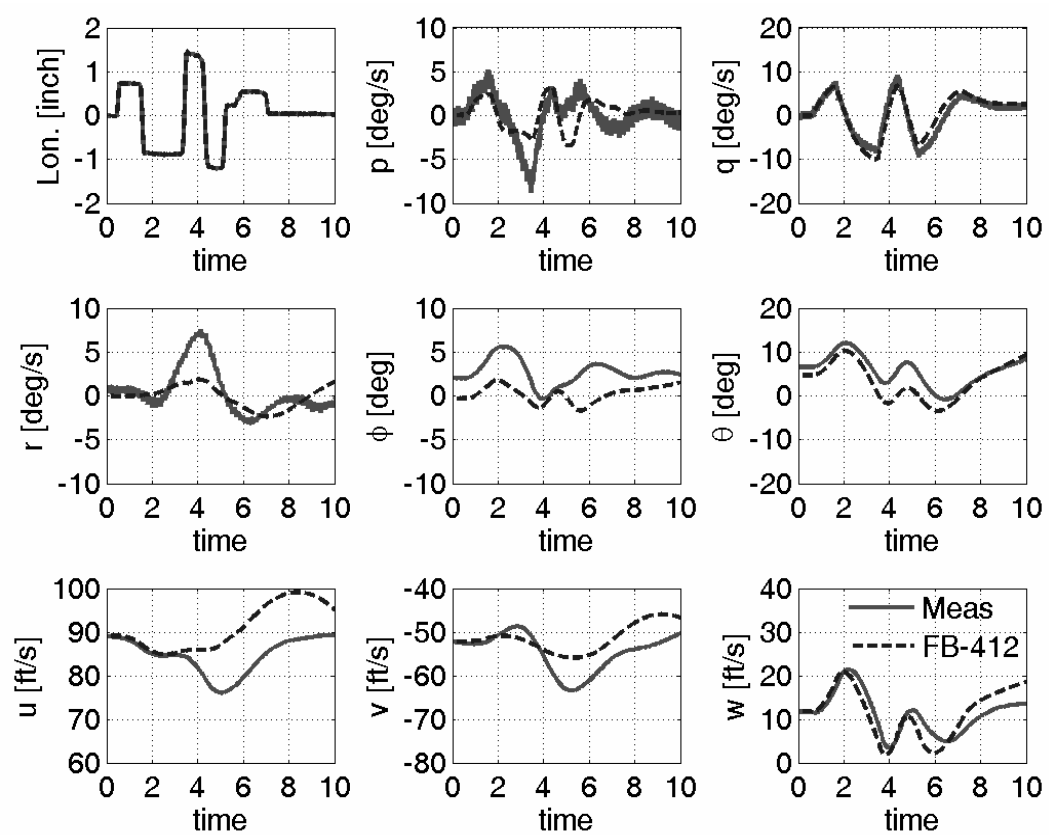


Figure 11. Dynamic response TAS 35kt – pitch input.

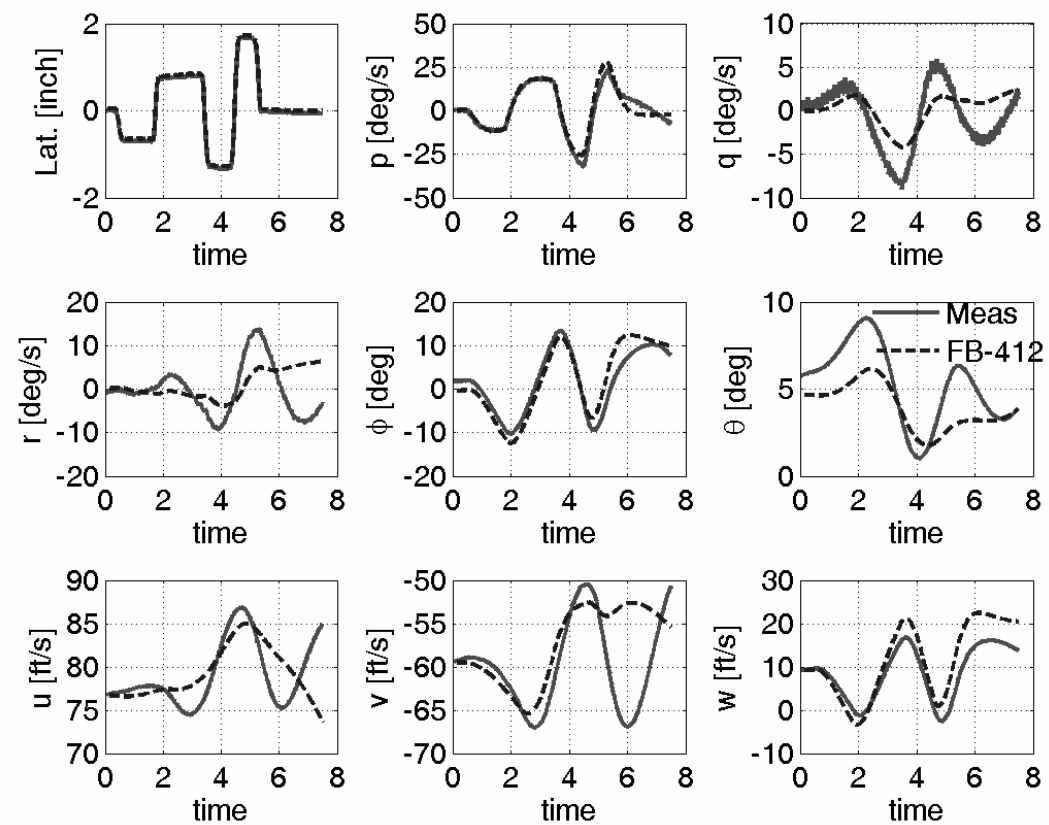


Figure 12. Dynamic response TAS 35kt – roll input.

https://doi.org/10.1017/S0001924000001780 Published online by Cambridge University Press

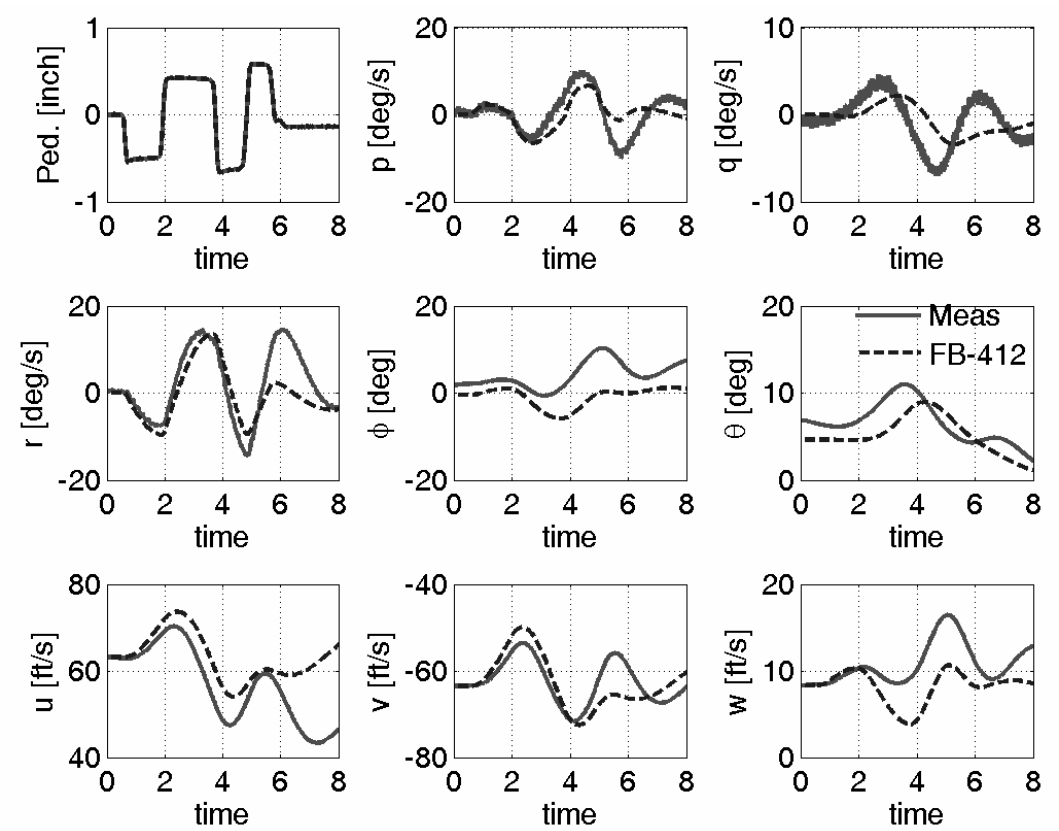


Figure 13. Dynamic response TAS 35kt – pedal input.

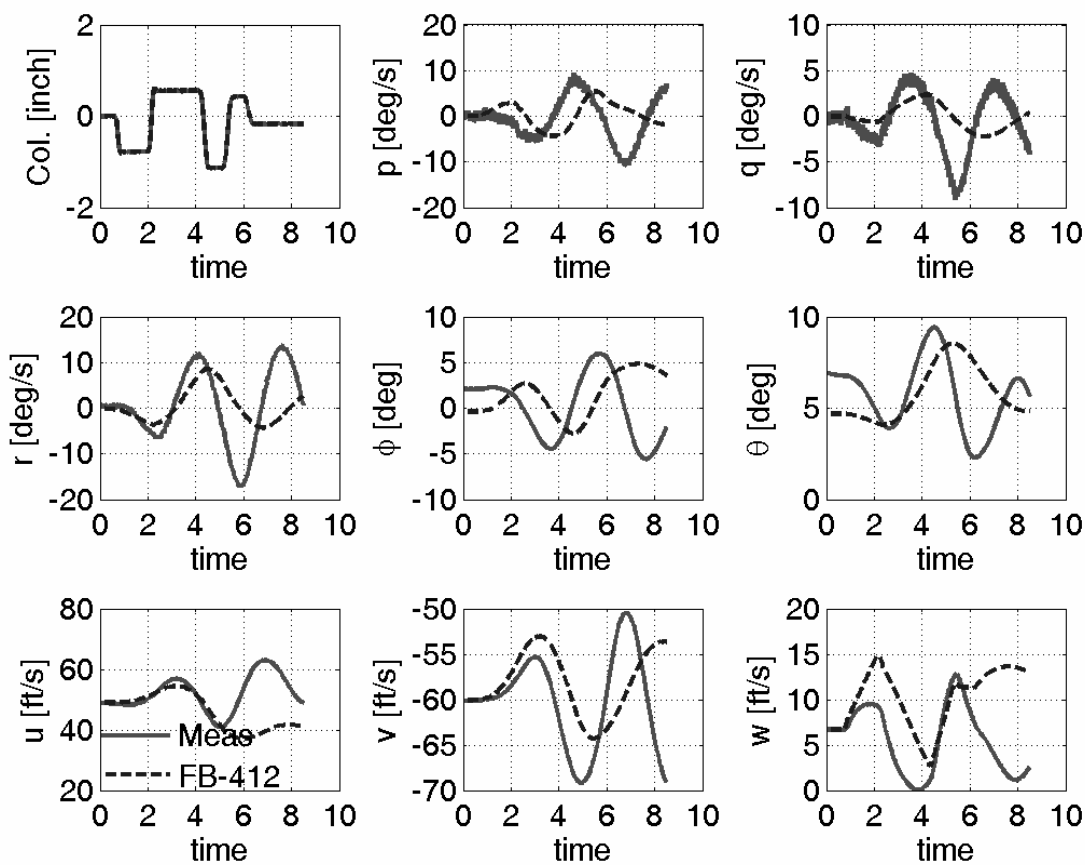


Figure 14. Dynamic response TAS 35kt – collective input.

https://doi.org/10.1017/S0001924000001780 Published online by Cambridge University Press

the opposite (incorrect) sense to the test data. The finite-state inflow model that includes the wake geometry distortion effect clearly improves the off-axis response. It may also be noted that excellent on-axis roll comparison is obtained for this flight condition. The yaw to roll coupling is also very well predicted by comparison to the flight-test data at 35kt.

Figure 16 shows the off-axis response to a pitch input at 18kt when wake distortion effect is included. Again, the cross-coupling (this time into roll) is predicted far better when the wake distortion effect is modelled.

12.0 CONCLUSIONS AND FUTURE WORK

The development and validation of a simulation model of the NRC Bell 412 in the FLIGHTLAB environment has been described. Overall, the base-line model gives excellent on-axis predictions compared to flight-test data over a broad speed range. It has been found that the pitch/roll off-axis responses in manoeuvres can be improved by including a wake geometry distortion effect in the Peters-He finite-state dynamic inflow model. Inclusion of unsteady (rotor) aerodynamics appears to have no significant effect on the flight mechanics. Including aerodynamic interference effects made noticeable differences in the trim pitch attitude prediction at low speeds. The principal remaining trim deficiencies are considered to be centred on the tail-plane modelling.

The F-B412 model is now being used as the basis for control law design work. Indeed, the first H-infinity optimal control law for the Bell 412, designed using this model, was successfully tested on the ASRA in December 2005 and results will be reported shortly.

One of the goals of the HELI-ACT project is to develop flight-envelope protection and structural load alleviation systems[33]. To pursue this goal further, models capable of predicting quantities such as pitch-link loads and blade bending moments will be required; these in turn are likely to require coupled flap, lag and torsional degrees of freedom, validated with appropriate flight-test data. This will be the subject of future work.

ACKNOWLEDGMENT

This research was part-funded by the U.K. Engineering and Physical Sciences Research Council through Research Grant GR/S42354/01.

REFERENCES

1. PADFIELD, G.D. and WHITE, M.D. Flight simulation in academia; HELIFLIGHT in its first year of operation, *Aeronaut J,* September 2003, **107**, (1075), pp 529-538.
2. GUBBELS, A.W. and CARIGNAN, S.J.R.P. The NRC Bell 412 Advanced system research aircraft – A new facility for airborne simulation, *Canadian Aero and Space J,* June 2000, **46,** (2), p 106-115.
3. DU VAL, R.W. A real-time multi-body dynamics architecture for rotorcraft simulation, Proceedings of the RAeS conference, 'The challenge of realistic rotorcraft simulation', London, UK, 7-8 November 2001.
4. CRESAP, W.L., and MYERS, A.W. Design and development of the Model 412 Helicopter, Proceedings of the American Helicopter Society 36th Annual Forum, May 1980.
5. YEN, J.G. and WELLER, W.H. Analysis and application of compliant rotor technology, 6th European rotorcraft and powered lift aircraft forum, Bristol, England, September 1980.
6. PETERS, D.A. and HE, CHENGJIAN. Finite state induced flow models part II: Three dimensional rotor disk, *J Aircr,* March-April 1995, **32,** (2).
7. PADFIELD, G.D. *Helicopter Flight Dynamics,* Blackwell Science, Oxford, 1996.
8. BRACKBILL, C.R. Helicopter Rotor Aeroelastic Analysis Using a Refined Elastomeric Damper Model, PhD Thesis in Aerospace Engineering submitted to the Pennsylvania State University, December 2000.
9. NAKADATE, M., TAGUCHI, H. and TAKAKI, J. Design and test evaluation of FBR bearingless main rotor, *J Ameri Heli Soc*, April 2001, **46,** (2).
10. NOONAN, K.W. Aerodynamic characteristics of two rotorcraft airfoils designed for application to inboard region of a main rotor blade, NASA TP-3009, July 1990.
11. DADONE, L.U. US Army helicopter design datcom volume 1 – airfoils, NASA-CR-153247, May 1976.
12. SCULLY, M.P.A. Method of computing helicopter vortex wake distortion, MIT Report ASRL TR138-1, June 1967.
13. BHAGWAT, M.J. and LEISHMAN, J.G. Rotor aerodynamics during manoeuvring flight using time accurate free-vortex wake, Proceedings of the American Helicopter Society 57th Annual Forum, May 2001.
14. JOHNSON, W. Wake model for helicopter in high speed flight, NASA CR-1177507, November 1988.
15. BAILEY, F.J. A simplified theoretical method of determining the characteristics of a lifting rotor in forward flight, NACA Report 716, 1941.
16. HARRIS, F.D., KOCUREK, J.D., MCLARTY, T.T. and TREPT, T.J. Helicopter performance methodology at Bell Helicopter Textron, Proceedings of the American Helicopter Society 35th Annual Forum, May 1979.
17. BIGGERS, J.C., MCCLOUD, J.L. and PATTERAKIS, P. Wind-tunnel tests of two full-scale helicopter fuselages, NASA TN D-1548, 1962.
18. WILSON, J.C. and MINECK, R.E. Wind-tunnel investigation of helicopter-rotor wake effects on three helicopter fuselage models, NASA TM X-3185, 1975.

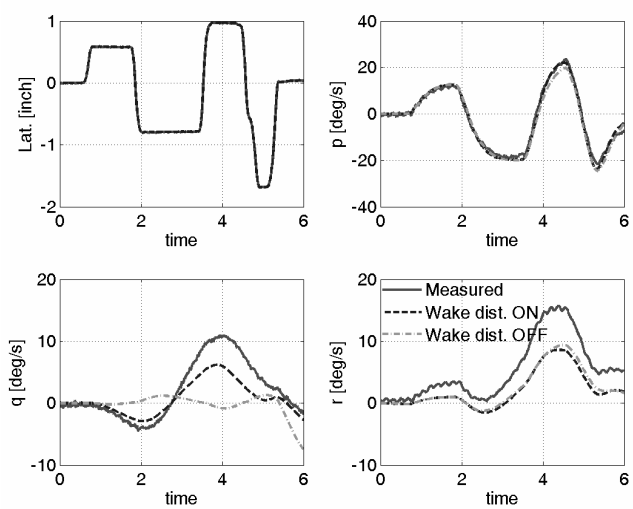


Figure 15. Roll to pitch coupling TAS 18kt with and without dynamic wake distortion effect.

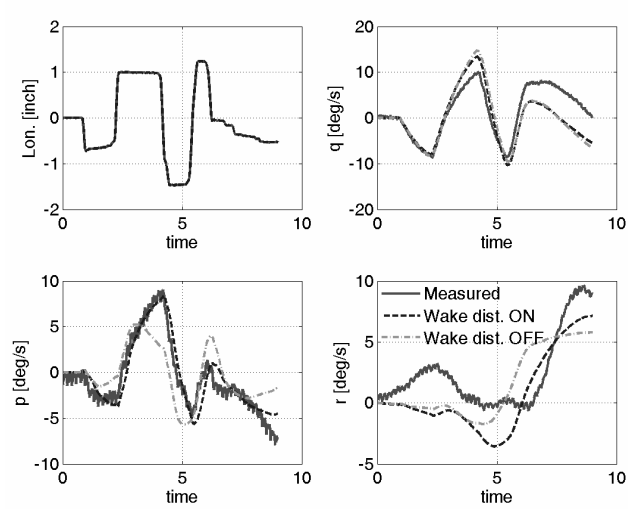


Figure 16. Pitch to roll coupling TAS 18kt with and without dynamic wake distortion effect.

https://doi.org/10.1017/S0001924000001780 Published online by Cambridge University Press

19. GUBBELS, A.W. and AURITI, L. NRC Bell 412 calibrations and aircraft design data, National Research Council of Canada. Flight Research Laboratory, Laboratory memorandum, LM-FRL-2004-0086, October 2004.
20. ANONYMOUS, Bell 412 EP product data. Bell Helicopter Textron, Fort Worth, October 2002.
21. KNIGHT, M., MONTGOMERY and WENZINGER, C.J. Wind-tunnel tests on a series of wing models through a large angle of attack range, Part I: force tests, NACA Report 317, 1930.
22. HOWLETT, J.J. UH-60A Black Hawk engineering simulation program: volume 1 – mathematical model, NASA-CR-166309.
23. HUI, K. Advanced modelling of the engine torque characteristics of a Bell 412 HP helicopter, American Institute of Aeronautics and Astronautics, AIAA-99-4110, 1999.
24. HE., CHENGJIAN Finite state dynamic wake interference modeling for rotorcraft simulation, American Helicopter Society, 53rd Annual Forum, Virginia Beach, VA, 29 April – 1 May, 1997.
25. GUBBELS, A.W. and ELLIS, D.K. NRC Bell 412 ASRA FBW systems description in ATA 100 format, Institute for Aerospace Research, National Research Council Canada, Report LTR-FR-163, April 2000.
26. BAILLIE, S., KERELIUK, S., MORGAN, J.M. and HUI, K. An evaluation of the dynamics and handling quality characteristics of the Bell 412 HP helicopter, *Canadian Aero and Space J,* March 1994, **40,** (1), pp 32-44.
27. ARNOLD, U.T.P., KELLER, J.D., CURTISS, H.C. and REICHERT, G. The effect of inflow models on the predicted responses of helicopters, *J Amer Heli Soc,* January 1998, **43,** (1), pp 25-36.
28. CURTISS, H.C. Aerodynamic models and the off-axis response, American Helicopter Society, 55th Annual Forum, Montreal, Canada, 1999.
29. SCHULEIN, G.J., TISCHLER, M.B., MANSUR, M.H. and ROSEN A. Validation of cross-coupling modeling improvements for UH-60 flight mechanics simulations, *J Amer Heli Soc,* July 2002, **47,** (3), pp 209-213.
30. HE, CHENGJIAN, LEE, C.S. and CHEN, WEIBIN Rotorcraft simulation model enhancement to support design, testing and operational analysis, *J Amer Heli Soc,* October 2000, **45,** (4), pp 284-292.
31. BROWN, R.E. Rotor wake modeling for flight dynamic simulation of helicopters, *AIAA J,* January 2000, **38,** (1), pp 57-63.
32. BAGAI, A. and LEISHMAN, J.G. Rotor free wake modeling using a pseudo-implicit technique-including comparison with experimental data, *J Amer Heli Soc,* July 1995, **40,** (3), pp 29-41.
33. VOSKUIJL, M., WALKER, D.J., MANIMALA B. and KUREEMUN, R. First step towards the design of an active pitch link load reduction system using novel control techniques, 31st European Rotorcraft Forum, Florence, Italy, 2005.

APPENDIX A: ROTOR PARAMETERS

Table A1
Key Bell 412 rotor parameters

Rotor parameters	Value
Rotor Radius, R	23ft
Mean blade chord, c	1·25 ft
Nominal rotor speed, Ω	33·93 rad/s
Blade mass, M_b	117lb
Flap hinge offset ratio, e_β	0·046
Flap first moment, M_β	51·44 slug-ft
Flap second moment, I_β	674·25 slug-ft^2
Flap spring stiffness, K_β	–15,381 lb-ft/rad
Lag hinge offset ratio, e_ζ	0·093
Lag first moment, M_ζ	44·24slug-ft
Lag second moment, I_ζ	571slug-ft^2
Lag spring stiffness, K_ζ	127,700lb-ft/rad
Lag damper coefficient, C_ζ	2,935ft-lb-s/rad

APPENDIX B: BODY AND WIND AXIS SYSTEM (RELATIVE TO BODY)

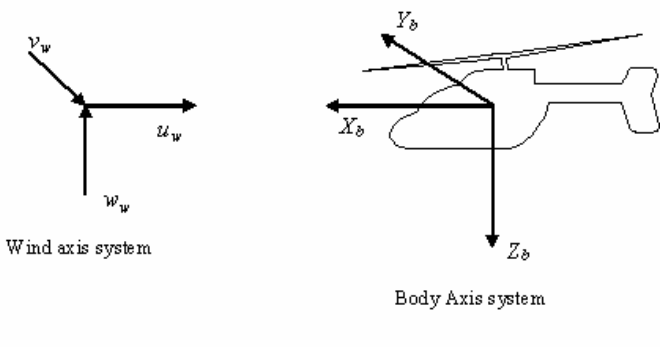


Figure B1. Body and relative wind axis

https://doi.org/10.1017/S0001924000001780 Published online by Cambridge University Press